MDPI

Article

Preparation and Characterization of Low-Carbon Cementitious Materials Based on Soda-Residue-Activated Ground Granulated Blast-Furnace Slag: A Case Study on Cemented Paste Backfills

Qiangsheng Ren [1], Wenyue Qi [1,*], Qingxin Zhao [1,2], Yali Jia [1], Yabin Feng [1], Yongji Han [1], Ge Duan [1] and Haotian Pang [1]

[1] Hebei Province Engineering Research Center for Harmless Synergistic Treatment and Recycling of Municipal Solid Waste, Yanshan University, Qinhuangdao 066004, China
[2] State Key Laboratory of Metastable Materials Science and Technology, Yanshan University, Qinhuangdao 066004, China
* Correspondence: wenyueqi@ysu.edu.cn

Abstract: To investigate the issues related to significant environmental damage and poor resource utilization of soda residue (SR), the composition and microstructure of hydration products of the GGBS (ground granulated blast-furnace slag) synergistically activated by NaOH-SR are characterized by an X-ray diffraction (XRD), Fourier-transform infrared spectrometry (FTIR), thermogravimetric–differential thermogravimetric (TG-DTG) analysis, and scanning electron microscope X-ray energy dispersive spectrometry (SEM-EDS). The effect of SR proportion, activator dosage, and water-to-binder ratio on the hydration process is studied. Results indicate that the hydration products mainly include hydrated calcium chloroaluminate ($3CaO \cdot Al_2O_3 \cdot CaCl_2 \cdot 10H_2O$, FS), hydrated calcium aluminosilicate ($Ca_2Al_3(SiO_4)_3OH$, C-A-S-H), halite (NaCl), calcite ($CaCO_3$), and C-S-H gel. With the increase in SR proportion (especially from 80% to 90%), the C-S-H gel yield decreases significantly, while the FS yield rapidly increases, and the T-O-Si (T = Al or Si) peak shifts to a higher wavenumber range (955 cm^{-1} to 975 cm^{-1}). With the decrease in activator dosage (40% to 15%), the hydration reaction gradually weakens, and the FTIR band of the T-O-Si (T = Al or Si) shifts to the lower wavenumber range (968 cm^{-1} to 955 cm^{-1}). Then, cemented paste backfills (CPBs) are prepared with iron tailings as the aggregate. At mass content of 75%, SR proportion of 80%, and activator dosage of 30%, the fluidity of the CPB reaches 267.5 mm with a 28-day unconfined compressive strength (UCS) of 2.4 MPa, confirming that SR- and NaOH-synergistically-activated GGBS has great application prospects in backfill mining.

Keywords: alkali-activated cementing material; paste backfill; hydration product; composition; microstructure

1. Introduction

Alkali-activated materials (AAM) refer to the materials which are made by reacting amorphous solid aluminosilicate with alkali activated agent [1]. They have excellent mechanical performance [2], low hydration heat [3], and strong resistance against chemical erosion [4]. Compared with ordinary Portland cement (OPC), its carbon footprint is 40–80% lower than that of similar of cement products [5]. This is mainly because 95% of the raw materials for AAM are industrial wastes, and its production does not require a "two grinding and one firing" process. The alkali-activated slag (AAS) reactions initiate with the cleavage of Si-O-Si and Al-O-Si bonds, through GGBS dissolution, creating a large number of unstable oligomeric aluminosilicate tetrahedral units. These units form a gelled and precipitated structure through dehydration, recombination, and polymerization [6]. The main AAS products are C-S-H gel with a low Ca/Si ratio [7,8]. Moreover, hydrotalcite

is uniformly mixed with C-S-H in MgO-containing GGBS and Al_2O_3-Fe_2O_3-monosulfate (AFm) [9]. Studies suggested that the typology and nature of the activating agent is a critical variable affecting the composition and morphology of hydration products.

Conventional activators include alkali and alkaline earth metal hydroxides, carbonates, sulfates, and silicates. Chen et al. [10] found that increasing alkaline contents and modulus promoted the development of C-A-S-H and hydrotalcite phases in silicate-activated slag, whereas excessive alkalinity inhibited the hydration product formation. Lei et al. [11] used AAS to solidify dredging sludge (DS) with high water content, revealing that a 1:4 ratio of sodium hydroxide to sodium silicate resulted in better curing, and the main hydration products are C-S-H gels. Ben Haha et al. [9] conducted tests of alkali activator (NaOH) and sodium silicate to activate GGBS with different Al_2O_3 contents, the main hydration products were aluminum-containing C-S-H and hydrotalcite phases, and the C-S-H of GGBS with low Al_2O_3 content was more fibrous at early age, while the C-S-H of GGBS with high Al_2O_3 content were closely arranged. Ma et al. [12] adopted Na_2CO_3 to replace some anhydrous Na_2SiO_3 to prepare a composite activator, irregular calcite particles with spindle, spherical and cubic shapes were formed with increasing Na_2CO_3 content, while the amounts of C-S-H and acicular gel products decreased. Rashad et al. [13] found that the hydration products of sodium sulfate-activated GGBS were mainly C-S-H, ettringite, and hydrotalcite. The ettringite with a hexagonal columnar structure also increased with sodium sulfate content. Jin and Al-Tabbaa [14] studied the effect of sodium carbonate and activated MgO to activate GGBS, and the main hydration products were C-S-H gel network, calcite, and hydrotalcite. Moreover, the density of C-S-H gel increased with the increase in Na_2CO_3 content. Chi and Huang [15] used liquid Na_2SiO_3 to activate GGBS and fly ash (FA), and the main hydration products were amorphous alkaline aluminum silicate with a three-dimensional gel-type zeolite structure, low-crystal hydrated calcium silicate gel with a trans-chain structure, and ettringite with a rod-like crystalline phase. Abdalqader et al. [16] found that the main reaction products of Na_2CO_3-activated FA/GGBS were C-(N)-A-S-H, hydrotalcite-like phase, calcite, and gaylussite. In a system containing GGBS alone, C-S-H gel exhibited a disordered riversideite-type structure. However, conventional alkaline activators are expensive and have high carbon emissions [17], limiting their large-scale engineering applications.

For more than the past 10 years, researchers have begun to replace traditional activators with alkaline wastes. Xu et al. [18] used ammonia soda slag (ASR), GGBS, steel slag, and desulfurized gypsum to prepare cementing materials. The increase in ASR content improved the hydration rate of cementing materials and increased NaCl, $CaCO_3$, and FS contents, while excess ASR enhanced the volume of harmful pores. Li and Yi [19] found that the alkaline environment provided by $Ca(OH)_2$ in carbide slag (CS) accelerated the hydration of GGBS and generated more C-S-H, C-A-H, C-A-S-H, AFt, AFm, and hydrotalcite phases, and yet the high content of crystalline $Ca(OH)_2$ decreased the amount of hydration products. He et al. [20] discussed the effects of SR, CS, and GGBS to reinforce dredged sediment. The increasing SR content facilitates the creation of ettringite and calcium chloroaluminate hydrate (FS), and the increase in CS content promoted the formation of gismondite. Sun et al. [21] indicated that the main products of white mud (WM) activation of GGBS/FA were C-A-S-H, calcite, and hydrotalcite. With the increase in WM content, more hydrotalcite was generated by the hydration reaction. Guo et al. [22] prepared AAM using SR and CS to synergistically activate GGBS and FA. As the CS content increased, more C-S-H gel, Friedel's salt (FS), and hydrotalcite contents were formed in hydration products. Prior research has focused on the macroscopic properties of cementitious materials with alkaline waste instead of traditional activator, and the development of microstructure and hydration products need to be further studied. Furthermore, the performance design of solid waste-based cementitious materials in practical engineering applications is also urgent to be resolved.

The paper is arranged as described below. The next section describes the experimental scheme, i.e., the raw and chemical materials used, the specimen preparation and mixing

ratios of the cement paste and the experimental scheme performed. This is then followed by a discussion of the hydration mechanism obtained from the XRD, FTIR, TG-DTG, and SEM-EDS test results. Next, a case study for the preparation of a CPB with the cemented paste and iron tailings aggregate was carried out. Lastly, the main conclusions are provided. It will provide the theoretical guidance for the utilization of industrial wastes in backfill engineering.

2. Materials and Methods

2.1. Materials

In this study, the materials were GGBS, SR, NaOH, and mixing water. A S95-grade GGBS was acquired from an ore powder factory in Qinhuangdao, China. SR was obtained from an alkaline factory in Tangshan, China. The SR was in the form of a slurry with a moisture content of more than 90%, and it was allowed to stand for 5–7 days before use. After removing the supernatant, the precipitated layer was dried, ground. NaOH was supplied by Qinhuangdao Zhisheng Trading Co., Ltd. (Qinhuangdao, China), and laboratory water from the tap is used as mixing water.

Particle size distribution, crystal structural, and chemical constituents of GGBS and SR were measured by BT-9300H laser diffraction particle size analyzer, XRD, and X-ray fluorescence (XRF) spectrum. The test results are shown in Figure 1 and Table 1. The chemical constituents of GGBS was CaO (31.30%), SiO_2 (35.20%), Al_2O_3 (17.60%), MgO (8.00%), SO_3 (3.00%), Na_2O (0.71%), Fe_2O_3 (0.79%), K_2O (0.57%), TiO_2 (2.32%), and others account for 0.51%. The predominant crystalline phase was quartz, while the curves showed an distinct peak at 20~40°, indicating a large amount of amorphous phase. The quality coefficient of GGBS $K = \frac{CaO+MgO+Al_2O_3}{SiO_2+MnO+TiO_2} = 1.517 \geq 1.2$ [22], indicated a high activity of GGBS. The average particle size of GGBS was 14.60 μm and the specific surface area was 461.1 m^2/kg. The predominant chemical composition of SR was CaO (40.30%), Cl (27.40%), SiO_2 (9.02%), Al_2O_3 (2.09%), MgO (10.00%), SO_3 (6.41%), Na_2O (3.58%), Fe_2O_3 (0.59%), K_2O (0.31%), and others account for 0.3%. The predominant crystalline phases were calcium chloride, gypsum, calcite, and rock salt phase, with an average particle size of 20.31 μm and a specific surface area of 261.2 m^2/kg.

**Table 1.** Chemical constituents of raw materials (wt/%), data from [23].

| Material	CaO	Al_2O_3	SiO_2	MgO	SO_3	Na_2O	Fe_2O_3	K_2O	TiO_2	P_2O_5	Cl	Other
GGBS	31.30	17.60	35.20	8.00	3.00	0.71	0.80	0.57	2.32	-	-	0.50
SR	40.30	2.09	9.02	10.00	6.41	3.58	0.59	0.31	-	-	27.40	0.30

2.2. Experimental Procedure

In this study, in order to focus on the hydration characteristics of the cementitious materials, a single net slurry system was prepared to facilitate microscopic testing. On the basis of the net slurry system, the optimal ratio of cementitious materials was selected to prepare a CPB, and the UCS and fluidity of the CPB are measured to evaluate the suitability of the cementitious materials. This will provide an important reference for the implementation of cementitious materials in backfill project.

The SR proportion, the activator dosage, and the water-to-binder ratio were evaluated as the influencing factors (Table 2). Firstly, the powder materials prepared by SR, NaOH, and GGBS was placed into the mixer for dry mixing, according to the mixing ratio. Then the pre-set volume of water was added to the dry mixture, continued wet mixing for 10 min. After stirring, the fresh mixture was poured into a triple test mold (20 mm × 20 mm × 20 mm) [24]. To ensure the mixing uniformity, the mold was filled three times. Each time 1/3 of the volume was filled, and the mold was shaken for a few seconds until the complete filling. After curing at RT (room temperature) (20–25 °C) for 24 h, we demolded and placed the specimen into a curing chamber at (20 ± 1) °C with humidity not less than 95% to obtain a cementing material test sample. Analyze the microstructure data, and then based on the

experimental results, a case study for the preparation of a CPB with the cemented paste and iron tailings aggregate was carried out. The CPB materials were prepared by mixing SR, NaOH, GGBS, iron tailings, and tap water according to the proportion of mixture, and were poured into a $70.7 \times 70.7 \times 70.7$ mm^3 tri-mold. Then, the specimens were demolded after maintained at RT for 48 h and placed in a curing chamber until the specified age to obtain the CPB test specimens.
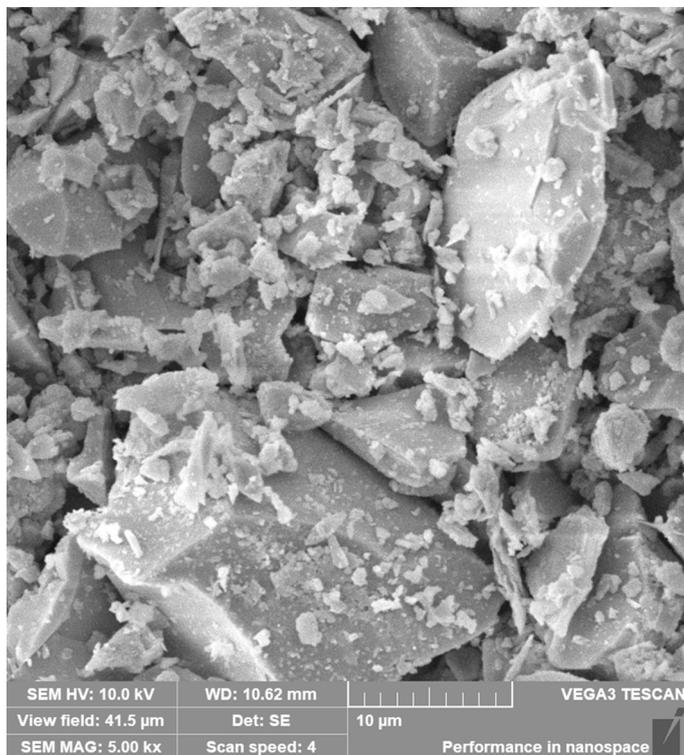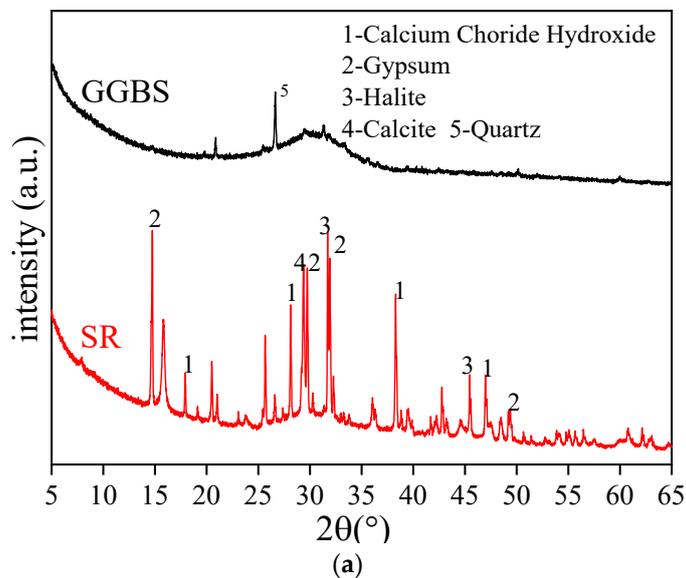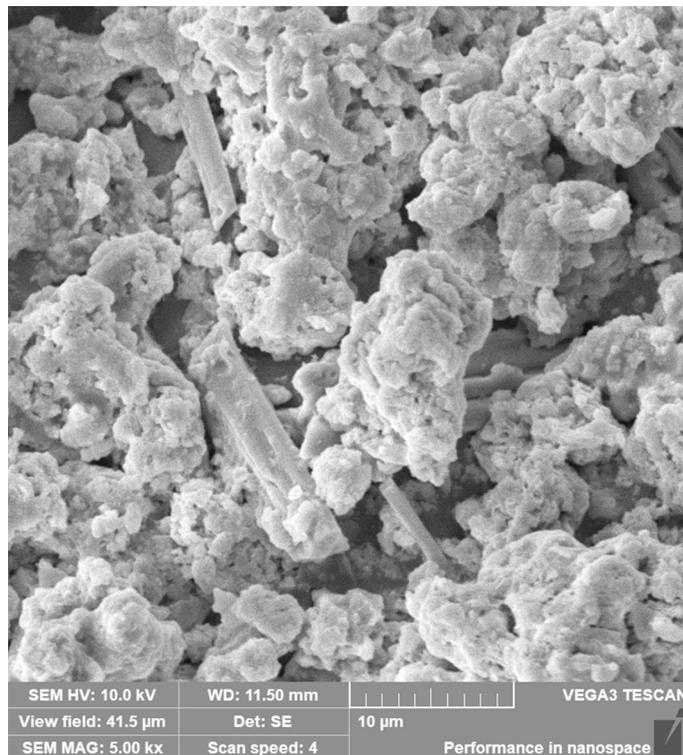
**Figure 1.** XRD spectra (**a**) of GGBS and SR versus SEM photos of (**b**) GGBS and (**c**) SR.

Table 2. The mix proportion.

Influence Factor	Specimen No.	W/C	Mix Proportion of Binders by Weight (%)			SR/Activator (%)	Cure Time
			GGBS	SR	SH		
SR/(SR + SH)	J-1	0.5	70	21	9	70	28 d
	J-2		70	22.5	7.5	75	
	J-3		70	24	6	80	
	J-4		70	25.5	4.5	85	
	J-5		70	27	3	90	
SR + SH	C-1	0.5	85	12	3	80	28 d
	C-2		80	16	4		
	C-3		75	20	5		
	C-4		70	24	6		
	C-5		65	28	7		
	C-6		60	32	8		
W/B	W-1	0.4	70	24	6	80	28 d
	W-2	0.5	70	24	6		
	W-3	0.6	70	24	6		
	W-4	0.7	70	24	6		

Note: The binder is GGBS, SH is sodium hydroxide (NaOH), W/B is the ratio of water-to-binder, (SR + SH) is the activator, SR/(SR + SH) is SR proportion.

2.3. Test Methods

Figure 2 describes the Mixing, casting and curing procedures of specimens. The cementitious material samples were pulverized into lumps and terminated the hydration reaction in isopropyl (C_3H_8O), dried and then crushed into powder. Subsequently, the crushed powder was sieved using a 200# sieve and the sieved powder was analyzed for microstructure and hydration composition.
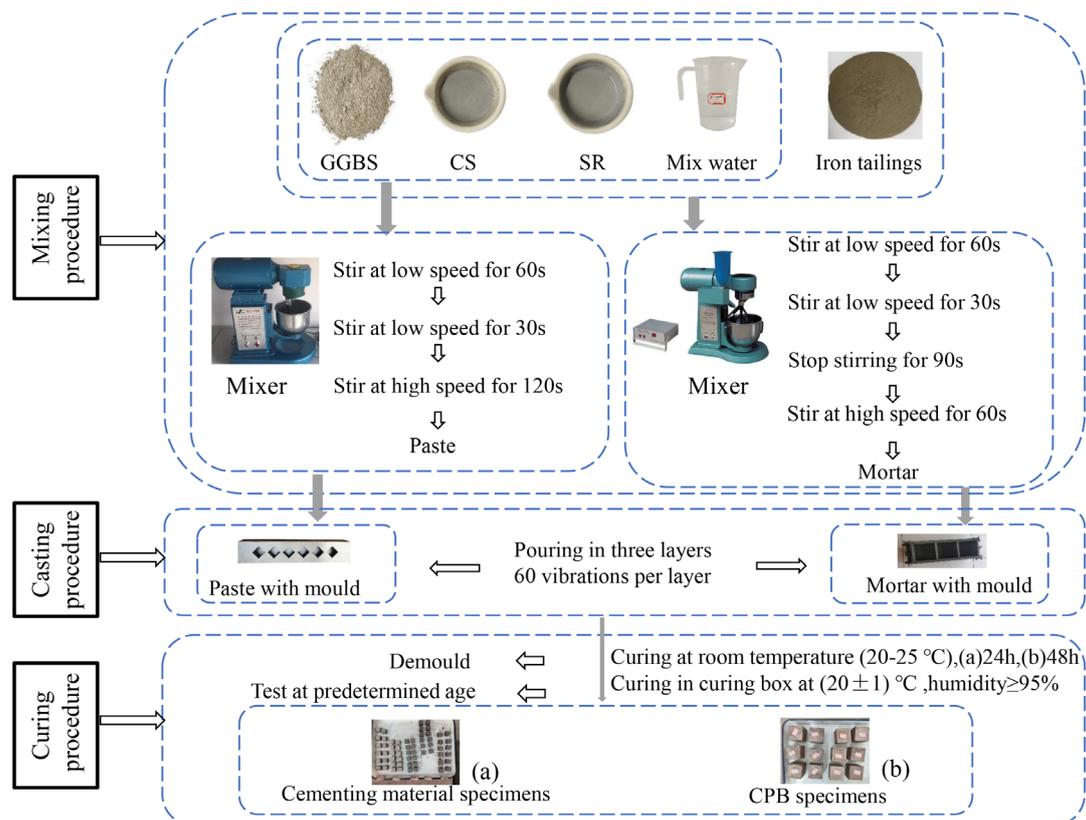
Figure 2. Mixing, casting, and curing procedures of specimens.

The D/MAX-2500/PC XRD was used for phase analysis. The tests were carried out using a copper target, a tube voltage and current of 40 kV and 40 mA respectively, and a scanning angle, speed and time of 5–65° and 2°/min for 30 min respectively. The STA449C/6/G simultaneous thermal analyzer was used for Weight-loss analysis. TG-DTG test with argon protection at a rate of 10 °C/min between the curing temperature of 20 °C and 1000 °C. Weight loss data analyzed by NETZSCH software. The E55 + FRA106 FTIR spectrometer was used to perform spectroscopic tests FTIR tests were carried out at a resolution of 2 cm^{-1} over a wavenumber range of 4000–400 cm^{-1}. The Czech VEGA3 XMU scanning electron microscope was used for microstructural analysis, aided by the determination of elemental composition using EDS. The INSTRON 5982 mechanical press with a load capacity of 50 kN was used to perform the UCS test with an average speed of 1 mm/min. Each group of specimens was tested three times at each age as experimental results. The truncated cone mould was used to test the fluidity of CPB slurry. Measure the CPB slurry diameter in both vertical directions using calipers and repeat three times.

3. Results and Discussion

3.1. XRD Analysis

Figure 3 shows that the hydration products formed by the SR-NaOH-synergistically-activated GGBS mainly include five typical crystal phases; hydrated calcium chloroaluminate ($3CaO \cdot Al_2O_3 \cdot CaCl_2 \cdot 10H_2O$, FS), hydrated calcium aluminosilicate ($Ca_2Al_3(SiO_4)_3OH$, C-A-S-H), sodium salt (NaCl), calcite ($CaCO_3$), and quartz (SiO_2). Among them, FS and C-A-S-H are the main crystalline products of the reaction [25]. The XRD shows a "hump" in the range of 20–40°, indicating the amorphous morphology of the C-S-H gel. In addition, diffraction peaks of $Ca_2Al_3(SiO_4)_3OH$ are visible, indicating that the dissolved free aluminum ions entered the C-S-H structure, generating C-A-S-H [19]. Quartz is mainly derived from the unreacted GGBS particles, while NaCl is associated with unreacted SR and the combination of free Na^+ and Cl^-.

With the increase in SR proportion, the diffraction peak intensity of FS and C-A-S-H increases, while the "hump" area decreases accordingly, suggesting that the quantities of produced C-S-H gels decreases. When the SR/(SR + SH) is 90%, a large number of FS is produced in the hydration reaction. However, when SR/(SR + SH) < 80%, the diffraction peak intensity decreases markedly, the diffraction peak of C-A-S-H gradually disappears, and the "hump" area remains unchanged. The reason is that excess OH^- inhibits the generation of C-S-H gel [22]. When the activator dosage is less than 20%, the SiO_2 diffraction peak intensity is higher, indicating more unreacted GGBS particles. The excessive amount of OH^- inhibits the formation of C-S-H gel when (SR + SH) > 35%, therefore, the diffraction peak intensities of FS and C-A-S-H are unchanged, and that of NaCl increases significantly due to more unreacted SR particles. The comparison indicates that the activator dosage ranging from 20% to 35%, that is the activator to binder ratio of 0.25–0.53 results in a more sufficient hydration reaction. When the water-to-binder ratio is range from 0.4 to 0.7, its effect on the diffraction peak intensity is insignificant, and the diffraction peak intensity of FS and C-A-S-H first increases and then decreases. When the water-to-binder ratio is 0.5, the diffraction peaks of FS and C-A-S-H and the "hump" area are relatively prominent. With the increasing of water-to-binder ratio, the hydration product gradually decreases, and a small amount of bleeding occurs.

1 $3CaO \cdot Al_2O_3 \cdot CaCl_2 \cdot 10H_2O$
2 NaCl
3 $CaCO_3$
4 SiO_2
5 C-A-S-H

(**a**)

1 $3CaO \cdot Al_2O_3 \cdot CaCl_2 \cdot 10H_2O$
2 NaCl
3 $CaCO_3$
4 SiO_2
5 C-A-S-H

(**b**)

1 $3CaO \cdot Al_2O_3 \cdot CaCl_2 \cdot 10H_2O$
2 NaCl
3 $CaCO_3$
4 SiO_2
5 C-A-S-H

(**c**)
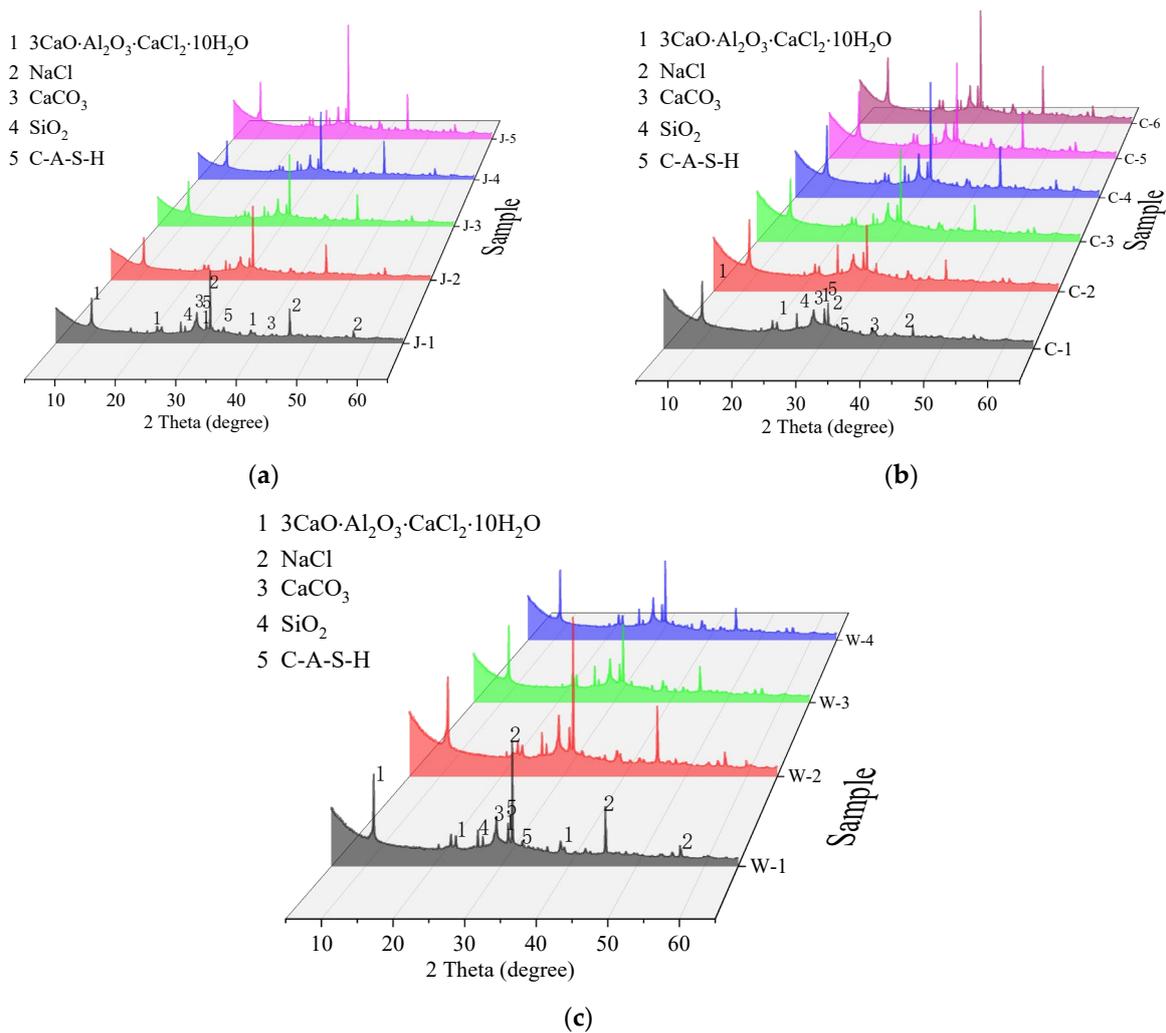
Figure 3. XRD patterns (**a**–**c**) of all 28 d net slurry specimens at different groups.

3.2. SEM Analysis

Figure 4 shows that the hydration products of the GGBS activated by SR-NaOH are mainly amorphous C-S-H gel. The C-S-H gel is formed by the accumulation of irregular-shaped gel units and is mostly arranged in a disordered state, such as flocculent and scaly. The particulate matter is C-A-S-H gel, with a relatively sparse distribution, and is mostly embedded on the C-S-H gel surface. The acicular rods, irregular flakes, and hexagonal flakes are mostly FS, distributed on the surface of amorphous products and interspersed in internal micro-cracks, playing the role of bridging and filling micro-cracks. With the increase in SR proportion, C-S-H gel breaks from a continuous lump structure into a dispersed fragment structure. Especially, when the SR proportion is higher than 80%, the number of pores increases significantly sticking with a large number of regular lamellar crystals cutting, indicating that the unreacted GGBS particles increases. Moreover, when the activator dosage is 15%, a number of hydration products are deposited on the surface of irregular GGBS particles, these particles bond with each other to form a flocculent network structure in a gel state. With the increase in the activator dosage, the hydration products fill the pores. Accordingly, the structure becomes continuous and dense, developing from the flocculent amorphous gel network to the film-like, lump-like continuous structure. When the activator dosage exceeds 35%, a large number of SR particles are formed that are not involved in the hydration reaction, and the surface of the gel structure is covered with a NaCl layer. In addition, the continuous lump structure of C-S-H gels formed under

different water–binder ratios is all relatively complete, while the density of the structure increases first and then decreases with the increase in the water–binder ratio.


(**a**) J-2 group

(**b**) J-3 group

(**c**) J-5 group
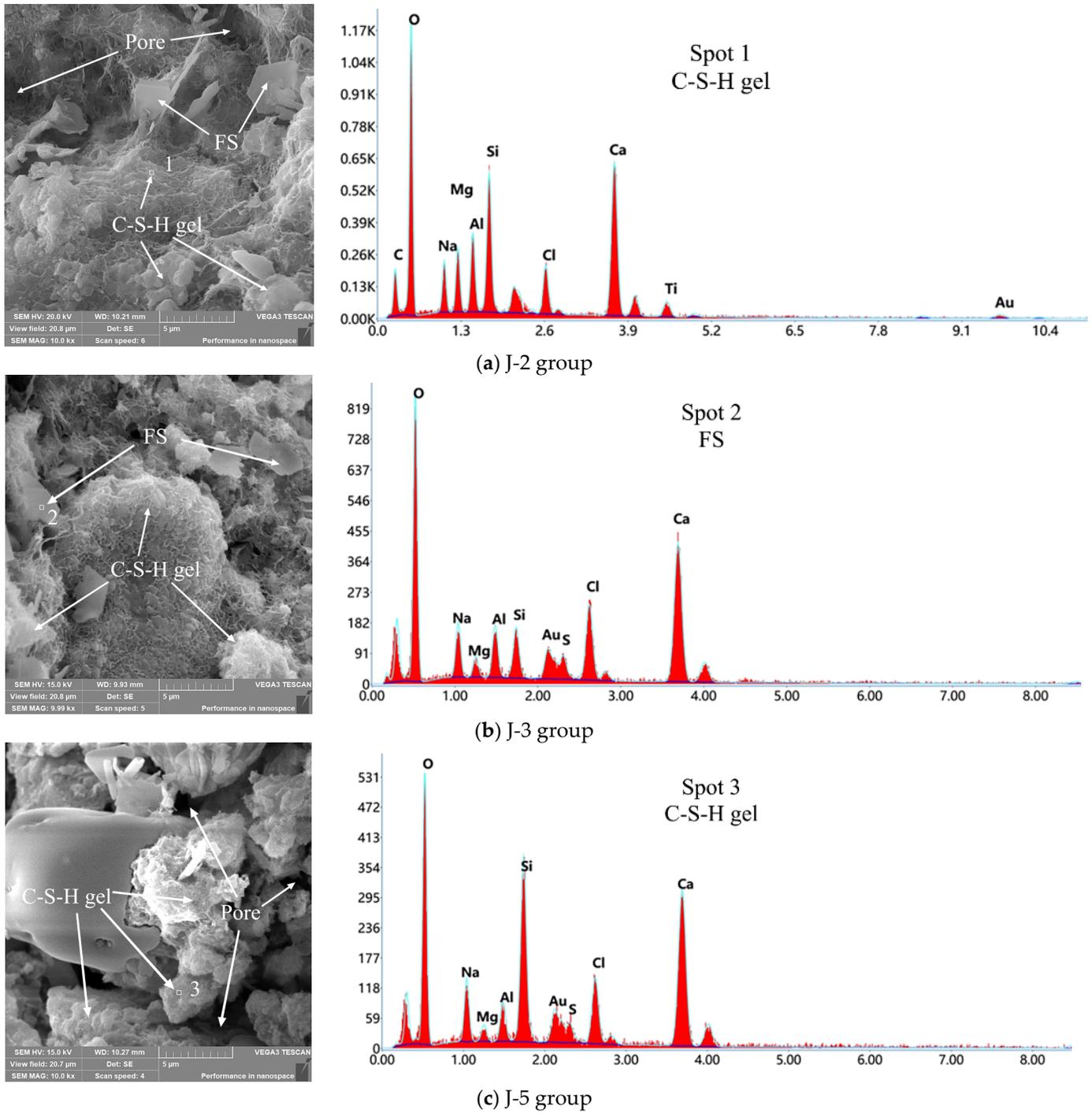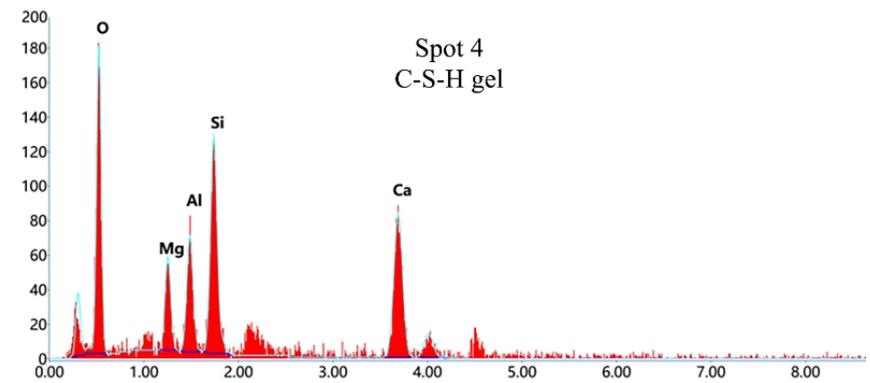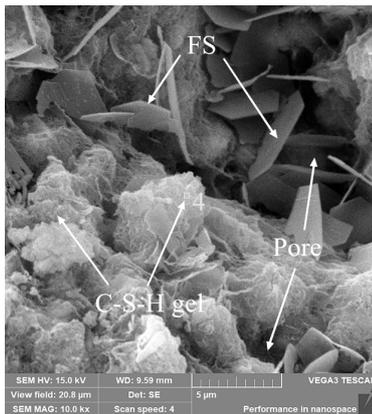
Figure 4. *Cont.*
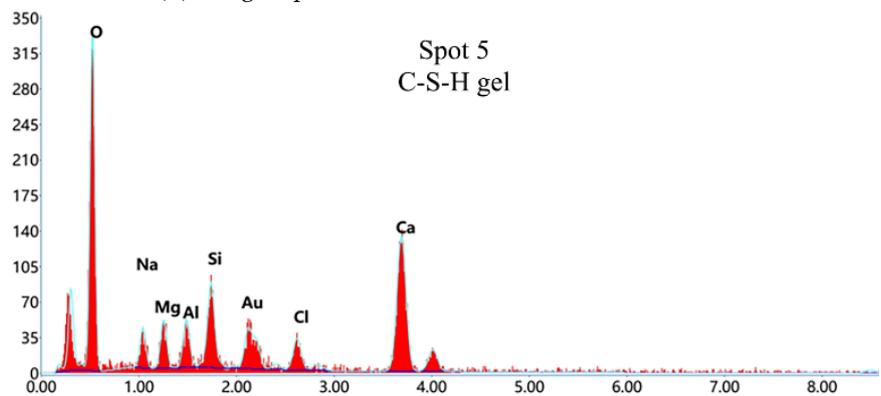
(**d**) C-1 group

(**e**) C-6 group
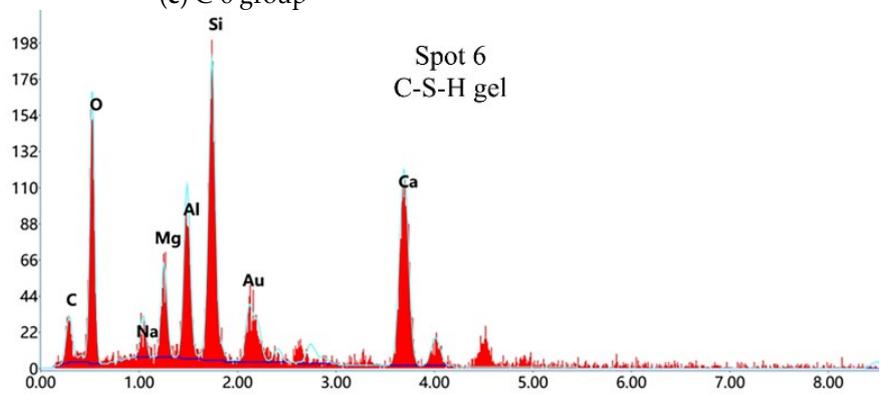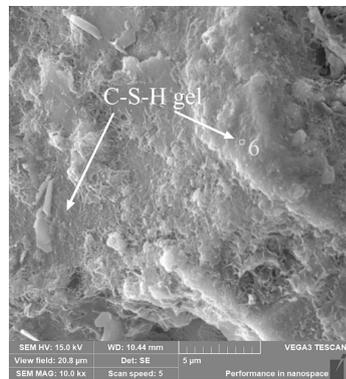
(**f**) W-1 group

(**g**) W-3 group

Figure 4. *Cont.*

**(h)** J group **(i)** C group **(j)** W group
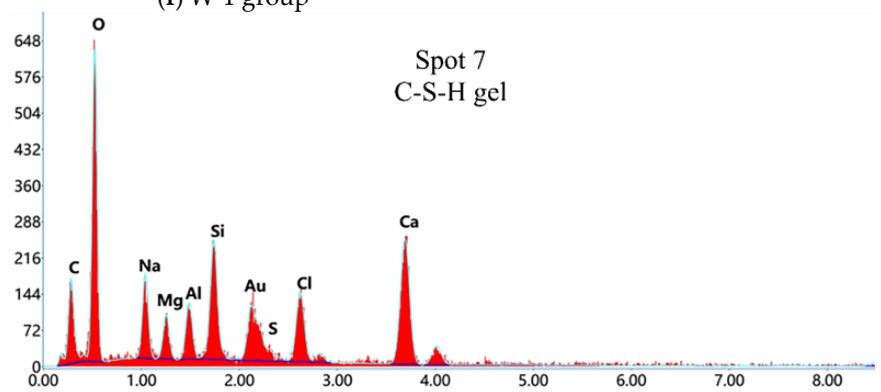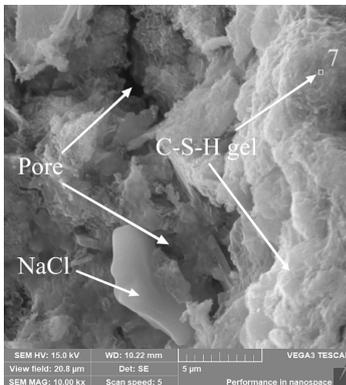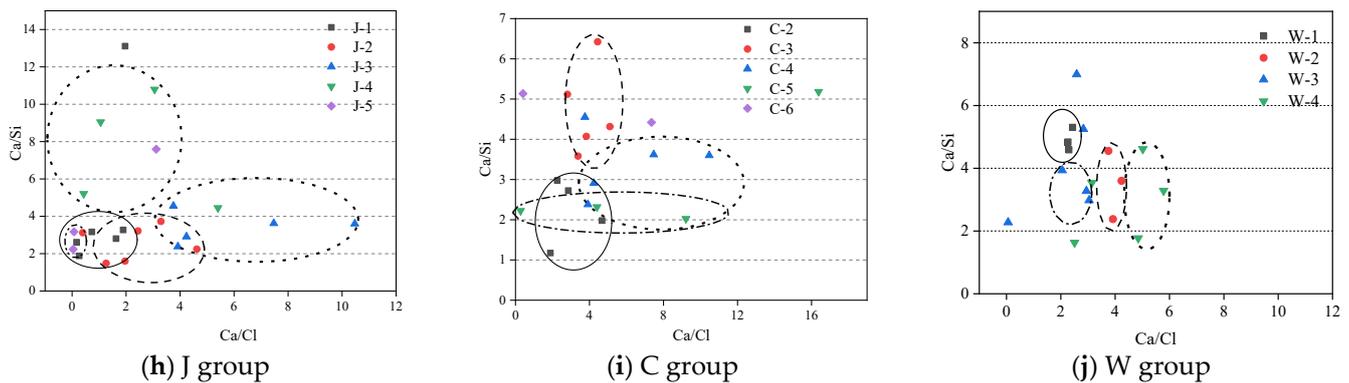
Figure 4. SEM images (**a**–**g**) and EDS results (**h**–**j**) of all 28 d net slurry specimens at different groups.

The EDS results of marked points are shown in Figure 4. Among them, Ca/Si of raw material GGBS is 2.24 and Ca/Al is 4.148, and the mean Ca/Si and Ca/Al in J-4 Spot 4, J-5 Spot 1, C1 Spot 3, and Spot 6 areas are 2.36 and 4.42, respectively, which are fitted with those in the raw material GGBS, suggesting that the corresponding material belongs to incompletely hydrated GGBS. The Ca/Si of SR is 5.918 and Ca/Cl is 1.007, the average Ca/Si in the C-6 Spot 2 area is 5.59, and a large amount of Cl existed, revealing that the corresponding matter is SR not involved in reaction. The C-5 Spot 2 area of the specimen contains a large number of Na and Cl, representing the NaCl crystals.

The normal Ca/Si range of C-S-H gel is in the range of 0.8 and 1.7. The flocculent network hydration products observed by SEM are mainly C-S-H gel, with the Ca/Si range between 1.17 and 5.59. In addition, most products contain Si-O-Al, higher Al element contents are found at J-4 Spot5, C-3 Spot3, W-1 Spot1, Spot4, W-3 Spot4, and W-4 Spot4, indicating a stacking morphology of C-A-S-H and C-S-H. The Ca/Cl ranges in J-2 Spot3, J-3 Spot2, and W-1 Spot2 areas are 2.27~3.92, and there is a certain amount of Si, indicating that FS shows surface adhesion phenomenon with C-S-H gel. When SR/(SR + SH) range is 70~80%, Ca/Cl in the substrate shows an increasing trend, and the main hydration product is C-S-H gel. When the SR proportion range further increases to 80~90%, the Ca/Si and FS content in the substrate increases significantly. When the activator dosage is 15%, a small amount of Cl element is detected, and the hydration product is mainly C-S-H gel. The GGBS is sufficiently hydrated at an activator dosage of 20~35%, in addition, the Ca/Si in the substrate shows an increasing trend as the activator dosage increases from 20% to 25% and decreases from 25% to 35%. When it reaches 40%, the Ca/Si in the substrate is between 5 and 6, and the Ca/Cl ratio is high, indicating existing un-hydrated SR particles. With increasing water-to-binder ratio, the fluctuations in Ca/Si and Ca/Cl in the substrate are lower, indicating that the water to-binder-ratio has a little effect on hydration products.

3.3. FTIR Analysis

Figure 5 shows that the absorption bands at (423,536) cm^{-1} correspond to the in-plane bending vibration and (779,972) cm^{-1} correspond to the tensile vibration of the Si-O bond, indicating the existence of C-S-H gel [26–28]. The absorption band near 878 cm^{-1} is caused by the bending vibration of CO_3^{2-} [29,30] and the absorption band at 1437 cm^{-1} is assigned to the symmetric stretching of C–O bonds [31], suggesting that calcite is formed. The absorption bands around 1632 cm^{-1} and 3483 cm^{-1} are attributed to hydroxyl groups of crystal water in C-S-H gel and FS crystal [25]. The absorption band in the range of 1300–800 cm^{-1} is assigned to the asymmetric stretching vibration of T-O-Si (T = Al or Si). When the activator dosage reduces from 40% to 15%, the intensity of the characteristic peaks of the C-S-H gels increased and the band shifts to a lower wavenumber range (968 cm^{-1} to 955 cm^{-1}). The reason is that more Al^{3+} ions or aluminate anions enter the silica network with the increase in the GGBS content. Since the force constant of the Si-O-Al bond is weaker than that of the Si-O-Si bond, the addition of Al^{3+} reduces the average bonding strength of Si-O-T, thereby reducing the asymmetric tensile vibration

frequency [32]. When the SR proportion increases from 70% to 90%, the band is shifted to a much upper wavenumber range (955 cm^{-1} to 975 cm^{-1}). The most plausible interpretation is that the band around 955 cm^{-1} is the overlapping of Cl$^-$ and C-S-H gel. At this time, the generated amount of FS salts ($3CaO \cdot Al_2O_3 \cdot CaCl_2 \cdot 10H_2O$) increases [33], produced by the reaction of chlorides in SR and active aluminates in pozzolanic matters [34] or generated by the combination of activated Al_2O_3 and CaO in GGBS with chloride in SR [35]. In addition, the characteristic peaks of C-S-H gel are most significant at a water–binder ratio of 0.5. These results consistent with the XRD and SEM-EDS analysis.
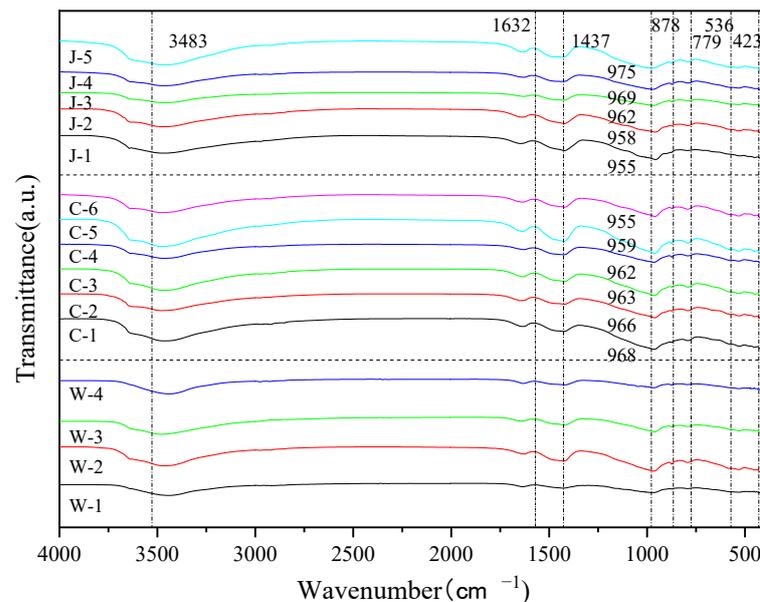

Figure 5. FTIR curves of all 28 d net slurry specimens at different groups.

3.4. TG-DTG Analysis

Figure 6 shows that the weight loss peak within 50–200 °C is attributed to the decomposition of C-S-H gel [9,36], corresponding to the evaporation of physically-bound water and the decomposition of gel products [37,38]. The weight loss in the 250–400 °C range is due to the desiccation of FS [39]. With the increase in SR proportion, the weight loss percent between 50–200 °C gradually decreases while it increases between 250–400 °C. When the SR proportion increases from 85% to 90%, the weight loss percent between 50–200 °C drops sharply by 13.9%, indicating a weakened hydration reaction and a significantly lower amount of generated C-S-H gel. With the increase in activator dosage, the weight losses between 50–200 °C and 250–400 °C show increasing trends. When the activator dosage increases from 15% to 20% and from 30% to 35%, respectively, the weight loss between 50 and 200 °C increases by 24.9% and 14.9%, indicating that the hydration reaction of GGBS generates more C-S-H gels when the activator dosage is higher than 20%. As the water to binder ratio changes from 0.4 to 0.7, the weight loss percent between 50–200 °C and 250–400 °C first increases and then decreases. When the water-to-binder ratio is 0.5, the C-S-H and FS show the highest weight loss percent, indicating that the SR-NaOH has a better synergistic activating effect on GGBS.
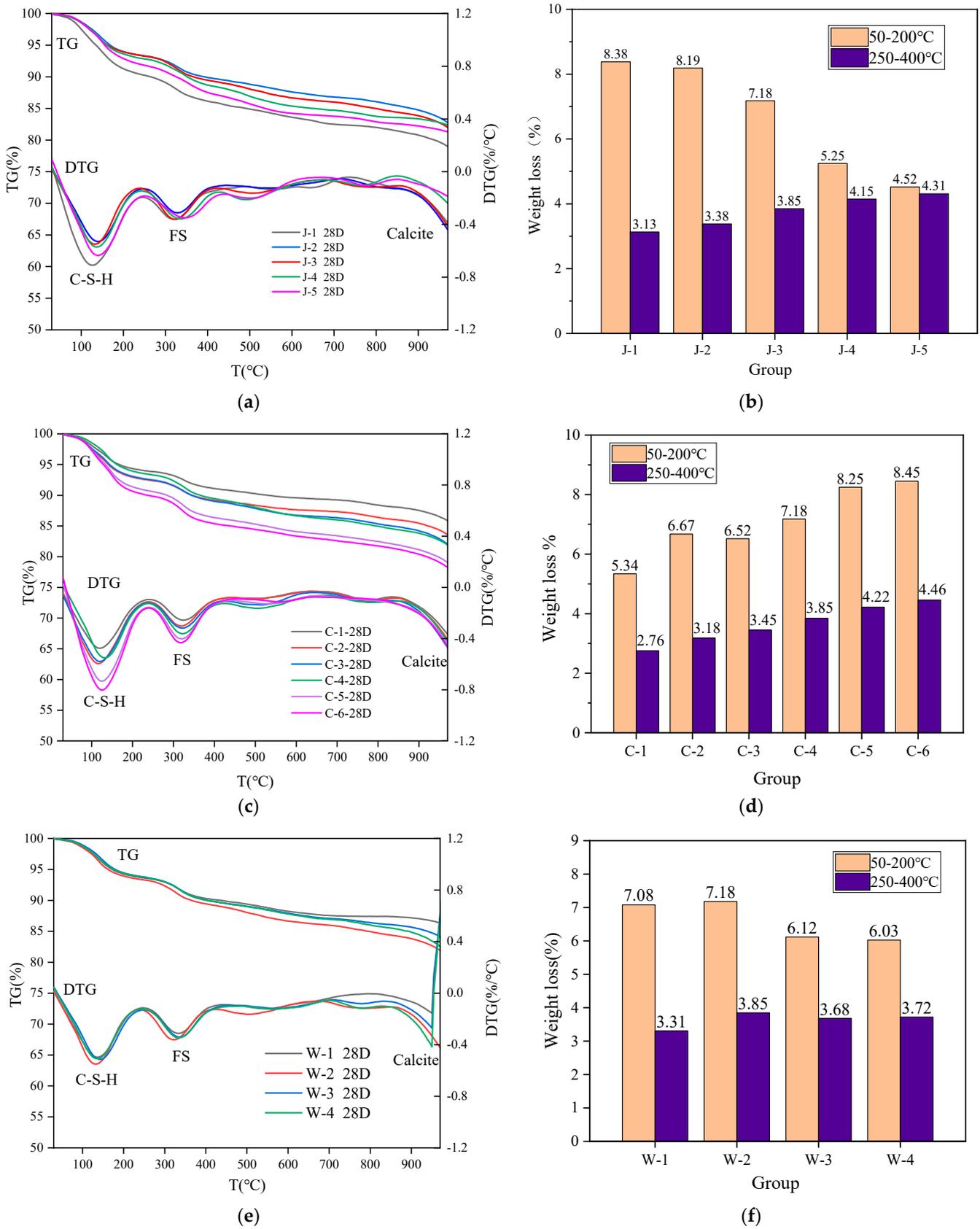
Figure 6. TG-DTG curves (**a**,**c**,**e**) and weight loss (**b**,**d**,**f**) of all 28 d specimens at different groups.

3.5. Discussion

The hydration process of composite cementitious materials is the result of the superposition of the hydration reactions of the components. SR slurry and NaOH together provide an alkaline environment for activating GGBS: C-S-H gels formed from NaOH activated GGBS, SR activated GGBS forming FS. When the SR proportion is 80%, this alkaline concentration ensures sufficient dissolution of GGBS to produce C-S-H gels, FS also increases with age, so the synergistic effect between the NaOH and SR improves the structural denseness. According to the test results, the water-to-binder ratio is 0.5, the SR proportion is 80%, and the activator dosage is 30% when the cementitious material has more abundant hydration products and dense microstructure, which greatly improves the pore structure. The experimental study of the hydration properties of the cementitious material was based on the net slurry system, and the correspondence of the performance between the net slurry system and the CPB materials still needs to be verified. The mechanical properties and fluidity of the CPB prepared by NaOH-SR-activated GGBS cementitious material determine whether it can be used in CPB engineering. Therefore, the water-to-binder ratio is 0.5, the SR proportion is 80%, and the activator dosage is 30% were used as the preferred targets for further testing of the CPB properties.

4. A Case-Study Preparation of CPB

CPB was prepared by adding iron tailings as aggregates on the basis of the above cementitious material ratios, and the chemical composition and particle size characteristics of iron tailings were consistent with the paper of Feng et al. [23]. The test protocols for the CPB specimens are presented in Table 3.

Table 3. Summary of the mix compositions of the CPB specimens prepared.

Trial Mix		Mass Content (%)	Activator Dosage (%)	SH (%)	SR (%)	Temp. (°C)	Mixing Water
Impact of Mass content	T-C-76	76	-	-	-	-	-
	T-C-75	75	30	20	80	20	tap water
	T-C-74	74	-	-	-	-	-
Impact of Activator dosage	T-A-20	-	20	-	-	-	-
	T-A-30	75	30	20	80	20	tap water
	T-A-35	-	35	-	-	-	-
Impact of SR proportion	T-N/A-70	-	-	30	70	-	-
	T-N/A-80	75	30	20	80	20	tap water
	T-N/A-90	-	-	10	90	-	-

Results and Discussion

The results for the fluidity of the CPB slurry and the UCS of the specimens for different Mass contents, Activator dosages, SR proportions are presented in Figure 7.

The possibility of the backfill mixture application is considered in terms of its full satisfaction with transportable requirements, which if non-compliant, can lead to blocking the mixture in the pipeline and an emergency situation [40]. Thus, the fluidity of the CPB slurry is commonly contained to be higher than 190 mm, and the 28-day UCS is generally controlled to be above 2 MPa [41,42]. As shown in (1), the fluidity of the CPB slurry gradually increases as the SR proportion decreases. When the proportion decreases from 90% to 70%, the fluidity increases from 245 mm to 282.5 mm, showing an increase of 13.3%. With the increase in the activator dosage, the fluidity of the slurry remains unchanged and above 250 mm. With the decrease in mass content, the fluidity increases gradually. When the mass content decreases from 76% to 74%, the liquidity increases sharply by 89.5 mm, showing an increasing trend reaching up to 33.3%.
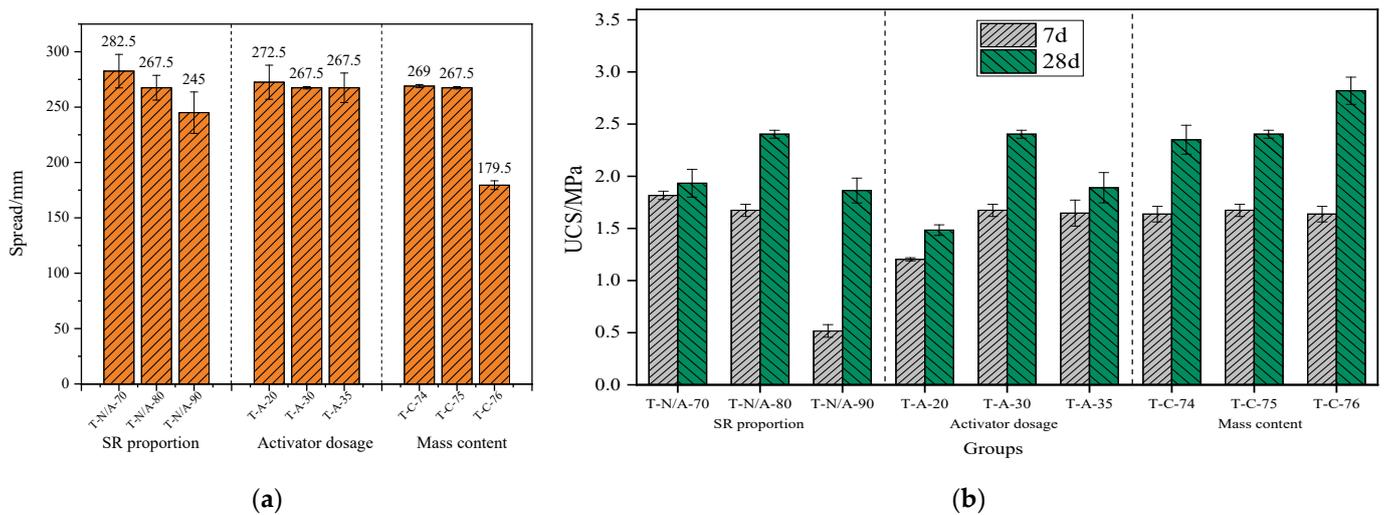
Figure 7. The influence rule of SR proportion, Activator dosage, and Mass content on the fluidity (**a**) and UCS (**b**) of CPB specimens.

(2) When the SR proportion is 90%, the UCS at 7-day was only 0.52 MPa; when the SR proportion is 80%, the UCS after 7 days and 28 days are 1.67 MPa and 2.4 MPa, respectively. When the SR proportion reduces from 80% to 70%, the 28-day compressive strength reduces from 2.4 MPa to 2.01 MPa, showing a decrease of 16.3%. When the activator dosage increases from 20% to 30%, the 28-day UCS increases from 1.47 MPa to 2.4 MPa, which showed an improvement of 63.3%. When dosage increases from 30% to 35%, the 28-day UCS shows a decreasing trend. When the mass content was increased from 74% to 76%, the UCS of the specimen increases. The 7-day UCS of all specimens is greater than 1.0 MPa, and the 28-day UCS of all specimens remains higher than 2.1 MPa, the 28-day UCS increases from 2.35 MPa to 2.82 MPa, which showed an increase of 20%.

5. Conclusions

1. Under the synergistic effect of NaOH-SR, the hydration products of GGBS were mainly C-S-H gel, C-A-S-H gel, and hydrated calcium chloroaluminate [$3CaO \cdot Al_2O_3 \cdot CaCl_2 \cdot 10H_2O$, FS]. With the increase in SR proportion, the hydration reaction weakens, the generated quantity of C-S-H gel reduces, and the generated FS content increases. When the SR proportion is 80%, the reaction of hydration of GGBS is much more adequate with the synergistic effect of NaOH and SR.

2. When the activator dosage is lower than 20%, more unreacted GGBS particles are found. When the activator dosage was more than 35%, excess OH^- inhibits the generation of C-S-H gel, and there were more SR particles and NaCl crystals that had not reacted. The reaction of hydration of GGBS is relatively adequate when the activator dosage is between 20% and 35%.

3. The GGBS synergistically reactivated by NaOH-SR is used as cementing materials, and iron tailings are used as aggregates to prepare the CPB. When the mass content is 75%, the SR proportion is 80%, and the activator dosage is 30%, the fluidity of the CPB prepared is 267.5 mm and a UCS of 2.4 MPa at 28 days. In this proportion of cemented filling material, both performance and cost aspects meet the requirements of the CPB.

Author Contributions: Q.R.: methodology, investigation, data curation, formal analysis, writing–original draft. W.Q.: conceptualization, resources, funding acquisition, writing—review and editing, project administration. Q.Z.: resources, writing—review and editing. Y.J.: resources, writing—review and editing. Y.F.: validation, data curation. Y.H.: validation, investigation. G.D.: validation, investigation. H.P.: validation, investigation. All authors have read and agreed to the published version of the manuscript.

Informed Consent Statement: Informed consent was obtained from all subjects involved in the study.

Data Availability Statement: Data are contained within the article.

Conflicts of Interest: The authors declare no conflict of interest.

References

1. Dener, M.; Karatas, M.; Mohabbi, M. High temperature resistance of self compacting alkali activated slag/portland cement composite using lightweight aggregate. *Constr. Build. Mater.* **2021**, *290*, 123250. [CrossRef]
2. Sun, J.; Zhang, Z.; Zhuang, S.; He, W. Hydration properties and microstructure characteristics of alkali–activated steel slag. *Constr. Build. Mater.* **2020**, *241*, 118141. [CrossRef]
3. Puertas, F.; Torres-Carrasco, M. Use of glass waste as an activator in the preparation of alkali-activated slag. Mechanical strength and paste characterisation. *Cem. Concr. Res.* **2014**, *57*, 95–104. [CrossRef]
4. Jiang, D.; Li, X.; Lv, Y.; Li, C.; Jiang, W.; Liu, Z.; Xu, J.; Zhou, Y.; Dan, J. Autogenous shrinkage and hydration property of alkali activated slag pastes containing superabsorbent polymer. *Cem. Concr. Res.* **2021**, *149*, 106581. [CrossRef]
5. Shariati, M.; Shariati, A.; Trung, N.T.; Shoaei, P.; Ameri, F.; Bahrami, N.; Zamanabadi, S.N. Alkali-activated slag (AAS) paste: Correlation between durability and microstructural characteristics. *Constr. Build. Mater.* **2021**, *267*, 120886. [CrossRef]
6. Le, T.-T.; Park, S.-S.; Lee, J.-C.; Lee, D.-E. Strength characteristics of spent coffee grounds and oyster shells cemented with GGBS-based alkaline-activated materials. *Constr. Build. Mater.* **2021**, *267*, 120986. [CrossRef]
7. Wang, S.-D.; Scrivener, K.L. 29Si and 27Al NMR study of alkali-activated slag. *Cem. Concr. Res.* **2003**, *33*, 769–774. [CrossRef]
8. Wang, S.-D.; Scrivener, K.L. Hydration products of alkali activated slag cement. *Cem. Concr. Res.* **1995**, *25*, 561–571. [CrossRef]
9. Ben Haha, M.; Le Saout, G.; Winnefeld, F.; Lothenbach, B. Influence of activator type on hydration kinetics, hydrate assemblage and microstructural development of alkali activated blast-furnace slags. *Cem. Concr. Res.* **2011**, *41*, 301–310. [CrossRef]
10. Chen, W.; Li, B.; Wang, J.; Thom, N. Effects of alkali dosage and silicate modulus on autogenous shrinkage of alkali-activated slag cement paste. *Cem. Concr. Res.* **2021**, *141*, 106322. [CrossRef]
11. Lang, L.; Chen, B.; Chen, B. Strength evolutions of varying water content-dredged sludge stabilized with alkali-activated ground granulated blast-furnace slag. *Constr. Build. Mater.* **2021**, *275*, 122111. [CrossRef]
12. Ma, C.; Zhao, B.; Guo, S.; Long, G.; Xie, Y. Properties and characterization of green one-part geopolymer activated by composite activators. *J. Clean. Prod.* **2019**, *220*, 188–199. [CrossRef]
13. Rashad, A.M.; Bai, Y.; Basheer, P.A.M.; Milestone, N.B.; Collier, N.C. Hydration and properties of sodium sulfate activated slag. *Cem. Concr. Compos.* **2013**, *37*, 20–29. [CrossRef]
14. Jin, F.; Al-Tabbaa, A. Strength and drying shrinkage of slag paste activated by sodium carbonate and reactive MgO. *Constr. Build. Mater.* **2015**, *81*, 58–65. [CrossRef]
15. Chi, M.; Huang, R. Binding mechanism and properties of alkali-activated fly ash/slag mortars. *Constr. Build. Mater.* **2013**, *40*, 291–298. [CrossRef]
16. Abdalqader, A.F.; Jin, F.; Al-Tabbaa, A. Development of greener alkali-activated cement: Utilisation of sodium carbonate for activating slag and fly ash mixtures. *J. Clean. Prod.* **2016**, *113*, 66–75. [CrossRef]
17. Zhao, D. Reactive MgO-modified slag-based binders for cemented paste backfill and potential heavy-metal leaching behavior. *Constr. Build. Mater.* **2021**, *298*, 123894. [CrossRef]
18. Xu, D.; Ni, W.; Wang, Q.; Xu, C.; Li, K. Ammonia-soda residue and metallurgical slags from iron and steel industries as cementitious materials for clinker-free concretes. *J. Clean. Prod.* **2021**, *307*, 127262. [CrossRef]
19. Li, W.; Yi, Y. Use of carbide slag from acetylene industry for activation of ground granulated blast-furnace slag. *Constr. Build. Mater.* **2020**, *238*, 117713. [CrossRef]
20. He, J.; Shi, X.-K.; Li, Z.-X.; Zhang, L.; Feng, X.-Y.; Zhou, L.-R. Strength properties of dredged soil at high water content treated with soda residue, carbide slag, and ground granulated blast furnace slag. *Constr. Build. Mater.* **2020**, *242*, 118126. [CrossRef]
21. Sun, R.; Fang, C.; Zhang, H.; Ling, Y.; Feng, J.; Qi, H.; Ge, Z. Chemo-mechanical properties of alkali-activated slag/fly ash paste incorporating white mud. *Constr. Build. Mater.* **2021**, *291*, 123312. [CrossRef]
22. Guo, W.; Zhang, Z.; Bai, Y.; Zhao, G.; Sang, Z.; Zhao, Q. Development and characterization of a new multi-strength level binder system using soda residue-carbide slag as composite activator. *Constr. Build. Mater.* **2021**, *291*, 123367. [CrossRef]
23. Feng, Y.; Qi, W.; Zhao, Q.; Huang, Y.; Ren, Q.; Qi, W.; Kong, F. Synthesis and characterization of cemented paste backfill: Reuse of multiple solid wastes. *J. Clean. Prod.* **2023**, *383*, 135376. [CrossRef]
24. Zhan, X.; Wang, L.; Wang, L.; Wang, X.; Gong, J.; Yang, L.; Bai, J. Enhanced geopolymeric co-disposal efficiency of heavy metals from MSWI fly ash and electrolytic manganese residue using complex alkaline and calcining pre-treatment. *Waste Manag.* **2019**, *98*, 135–143. [CrossRef] [PubMed]

25. Guo, W.; Wang, S.; Xu, Z.; Zhang, Z.; Zhang, C.; Bai, Y.; Zhao, Q. Mechanical performance and microstructure improvement of soda residue–carbide slag–ground granulated blast furnace slag binder by optimizing its preparation process and curing method. *Constr. Build. Mater.* **2021**, *302*, 124403. [CrossRef]

26. Mollah, M.Y.A.; Yu, W.; Schennach, R.; Cocke, D.L. A Fourier transform infrared spectroscopic investigation of the early hydration of Portland cement and the influence of sodium lignosulfonate. *Cem. Concr. Res.* **2000**, *30*, 267–273. [CrossRef]

27. Yu, P.; Kirkpatrick, R.J.; Poe, B.; McMillan, P.F.; Cong, X. Structure of Calcium Silicate Hydrate (C-S-H): Near-, Mid-, and Far-Infrared Spectroscopy. *J. Am. Ceram. Soc.* **2004**, *82*, 742–748. [CrossRef]

28. Petlovanyi, M.V.; Zubko, S.A.; Popovych, V.V.; Sai, K.S. Physicochemical mechanism of structure formation and strengthening in the backfill massif when filling underground cavities. *Vopr. Khimii I Khimicheskoi Tekhnologii* **2020**, *6*, 142–150. [CrossRef]

29. Tian, Z.; Ye, H. Electrical resistivity of partially-saturated alkali-activated slag containing sodium nitrite admixture. *Cem. Concr. Compos.* **2021**, *120*, 104053. [CrossRef]

30. Reig, F. FTIR quantitative analysis of calcium carbonate (calcite) and silica (quartz) mixtures using the constant ratio method. Application to geological samples. *Talanta* **2002**, *58*, 811–821. [CrossRef]

31. García Lodeiro, I.; Macphee, D.E.; Palomo, A.; Fernández-Jiménez, A. Effect of alkalis on fresh C–S–H gels. FTIR analysis. *Cem. Concr. Res.* **2009**, *39*, 147–153. [CrossRef]

32. Gu, Y.-M.; Fang, Y.-H.; You, D.; Gong, Y.-F.; Zhu, C.-H. Properties and microstructure of alkali-activated slag cement cured at below- and about-normal temperature. *Constr. Build. Mater.* **2015**, *79*, 1–8. [CrossRef]

33. Lin, Y.; Xu, D.; Zhao, X. Effect of Soda Residue Addition and Its Chemical Composition on Physical Properties and Hydration Products of Soda Residue-Activated Slag Cementitious Materials. *Materials* **2020**, *13*, 1789. [CrossRef] [PubMed]

34. Ubbrìaco, P.; Calabrese, D. Hydration Behaviour of Mixtures of Cement and Fly Ash with High Sulphate and Chloride Content. *J. Therm. Anal. Calorim.* **2000**, *61*, 615–623. [CrossRef]

35. Cheng, Y.; Li, Z.-G.; Huang, X.; Bai, X.-H. Effect of Friedel's salt on strength enhancement of stabilized chloride saline soil. *J. Cent. South Univ.* **2017**, *24*, 937–946. [CrossRef]

36. Zhang, J.; Tan, H.; He, X.; Yang, W.; Deng, X. Utilization of carbide slag-granulated blast furnace slag system by wet grinding as low carbon cementitious materials. *Constr. Build. Mater.* **2020**, *249*, 118763. [CrossRef]

37. Ismail, I.; Bernal, S.A.; Provis, J.L.; San Nicolas, R.; Hamdan, S.; van Deventer, J.S.J. Modification of phase evolution in alkali-activated blast furnace slag by the incorporation of fly ash. *Cem. Concr. Compos.* **2014**, *45*, 125–135. [CrossRef]

38. Gao, X.; Yu, Q.L.; Brouwers, H.J.H. Reaction kinetics, gel character and strength of ambient temperature cured alkali activated slag–fly ash blends. *Constr. Build. Mater.* **2015**, *80*, 105–115. [CrossRef]

39. Wang, Q.; Li, J.; Yao, G.; Zhu, X.; Hu, S.; Qiu, J.; Chen, P.; Lyu, X. Characterization of the mechanical properties and microcosmic mechanism of Portland cement prepared with soda residue. *Constr. Build. Mater.* **2020**, *241*, 117994. [CrossRef]

40. Petlovanyi, M.; Mamaikin, O. Assessment of an expediency of binder material mechanical activation in cemented rockfill. *J. Eng. Appl. Sci.* **2019**, *14*, 3492–3503.

41. Xue, G.; Yilmaz, E.; Song, W.; Cao, S. Compressive Strength Characteristics of Cemented Tailings Backfill with Alkali-Activated Slag. *Appl. Sci.* **2018**, *8*, 1573. [CrossRef]

42. Wang, S.; Song, X.; Wei, M.; Liu, W.; Wang, X.; Ke, Y.; Tao, T. Strength characteristics and microstructure evolution of cemented tailings backfill with rice straw ash as an alternative binder. *Constr. Build. Mater.* **2021**, *297*, 123780. [CrossRef]